

Role of dipolar and exchange interactions in the positions and widths of EPR transitions for the single-molecule magnets Fe_8 and Mn_{12}

Kyungwha Park^{1,2,*}, M. A. Novotny^{3,†}, N. S. Dalal^{2,‡}, S. Hill^{4,§}, and P. A. Rikvold^{1,5,||}

¹*School of Computational Science and Information Technology, Florida State University, Tallahassee, Florida 32306*

²*Department of Chemistry and Biochemistry, Florida State University, Tallahassee, Florida 32306*

³*Department of Physics and Astronomy, Mississippi State University, Mississippi State, Mississippi 39762*

⁴*Department of Physics, University of Florida, Gainesville, Florida 32611*

⁵*Center for Materials Research and Technology and Department of Physics, Florida State University, Tallahassee, Florida 32306*

(December 2, 2024)

Abstract

We examine quantitatively the temperature dependence of the linewidths and line shifts in electron paramagnetic resonance experiments on single crystals of the single-molecule magnets Fe_8 and Mn_{12} , at fixed frequency, with an applied magnetic field along the easy axis. We include inter-molecular spin-spin interactions (dipolar and exchange) and distributions in both the uniaxial anisotropy parameter D and the Landé g -factor. The temperature dependence of the linewidths and the line shifts are mainly caused by the spin-spin interactions. For Fe_8 and Mn_{12} , the temperature dependence of the calculated line shifts and linewidths agree well with the trends of the experimental data. The linewidths for Fe_8 reveal a stronger temperature dependence than those for Mn_{12} , because for Mn_{12} a much wider distribution in D overshadows the temperature dependence of the spin-spin interactions. For Fe_8 , the line-shift analysis suggests two competing interactions: a weak ferromagnetic exchange coupling between neighboring molecules and a longer-ranged dipolar interaction. This result could have implications for ordering in Fe_8 at low temperatures.

PACS numbers: 75.50.Xx, 76.30.-v, 75.45.+j

I. INTRODUCTION

Single-molecule magnets consist of identical molecules, each of which made up of several magnetic ions surrounded by many different species of atoms. A single molecule of the molecular nanomagnets Mn_{12} -acetate¹ and Fe_8 ² has an effective ground-state spin of $S = 10$ and a strong crystal-field anisotropy. A zero-field energy barrier against magnetization reversal is approximately 65 K (30 K) for uniaxial Mn_{12} (biaxial Fe_8).^{3–7} Despite their large effective spin, these single-molecule magnets have shown quantum coherence^{8,9} and quantum tunneling between the energy levels of the two potential wells.^{9–11} Although dipolar interactions between different molecules are weak, in the low-temperature limit and near zero applied field, a dipolar interaction could stimulate the quantum tunneling and thus explain the non-exponential magnetization relaxation observed at early times.^{12–17}

Recently, electron paramagnetic resonance (EPR) experiments on single crystals of Fe_8 and Mn_{12} have revealed interesting effects in the widths and positions of the EPR peaks as functions of energy level, resonance frequency, and temperature when the applied field is along the easy axis.^{4,18–21} For both Fe_8 and Mn_{12} , at fixed frequency, the linewidths increase with decreasing energy levels (the maximum linewidth corresponds to the transition between the ground state and the first excited state), and for a particular transition the linewidths increase with decreasing frequency. The temperature dependence of the linewidths for Fe_8 is quite different from that for Mn_{12} . For Mn_{12} , the linewidths increase smoothly with increasing temperature, showing a rather weak temperature dependence. For Fe_8 , for transitions at low resonant fields, the linewidths increase sharply with temperature at low temperatures, reach a maximum, and then decrease slowly with temperature at higher temperatures. The exception is the transition associated with the ground state, for which the linewidth decreases with increasing temperature in the whole temperature range studied (2–50 K). On the other hand, for the transitions with high resonant fields, the linewidths increase monotonically with increasing temperature. For Fe_8 , the line positions change non-monotonically with temperature.

The energy level and frequency dependence of the linewidths show that for both Fe_8 and Mn_{12} the distribution in the uniaxial anisotropy parameter D of the single-spin Hamiltonian, caused by defects in the samples, contributes substantially to the inhomogeneous linewidths.²⁰ This was also recently supported by terahertz spectroscopy for Mn_{12} .²² The microscopic origin of the distribution in D has not yet been fully understood.^{23,24} The analysis further show that for Fe_8 the dipolar interactions between molecules contribute to the linewidths as significantly as the distribution in D , while for Mn_{12} their contribution is less significant.²⁰ In a recent millimeter-wave experiment for Fe_8 ,²⁵ the dipolar field may have been overestimated because the distribution in D was not included.

Inspired by the experimental data on the temperature dependence of the linewidths and line positions, we here address the following two issues: (i) What causes the linewidths and line positions to depend on temperature for Fe_8 and Mn_{12} ? (ii) Why is the temperature dependence of the linewidths for Fe_8 different from that for Mn_{12} ? We attempt to answer these questions by providing a quantitative analysis of the linewidths and the line shifts vs temperature at fixed frequency, taking into account the spin-spin interactions (exchange and dipolar interactions) between different molecules, as well as distributions in the uniaxial anisotropy parameter D and the Landé g -factor.²⁰

This paper is organized as follows. A brief summary of the experimental procedures is presented in Sec. II. The models for Fe_8 and Mn_{12} are described separately in Sec. III. Our calculated linewidths and line shifts are presented vs temperature and discussed in comparison with the experimental data in Sec. IV. Our conclusions are provided in Sec. V.

II. SUMMARY OF EXPERIMENTAL PROCEDURES

All of the EPR experiments were performed on single crystals with the magnetic field aligned along or close to the direction of the easy magnetization axis, in a temperature range from 2 K to 50 K. For Mn_{12} , this direction coincides with that of the longest dimension of the essentially needle-shaped crystals. For Fe_8 , the direction was determined by measurement of the largest spread of the resonant field, by rotating the crystal around the approximately known orientation of the easy axis. The single crystals were prepared as described by Perenboom et al.^{4,5} and Achey et al.^{26–28} EPR measurements were made in the 100–190 GHz range with a resonant microwave cavity system described by Hill et al.²⁹, which enables observation of distortion-free EPR line shapes. The linewidths were determined by computer-fitting of the observed experimental spectra to either a Gaussian or a Lorentzian function for the spectra obtained at various temperatures. All the spectra were obtained by keeping the frequency fixed and sweeping the field to obtain the resonance peaks, as is usual in EPR spectroscopy.³⁰

III. MODEL

For the examined single-crystal sample of Fe_8 ,²¹ there are two sources of the EPR line *shifts*: temperature dependence of D and the electronic spin-spin interactions (dipolar and exchange interactions) between different molecules. There are also two sources of the EPR line *broadening*: the D -strain effect (distribution in D) and the spin-spin interactions.²⁰ For the examined Mn_{12} sample,²¹ the sources of the line broadening are the D -strain, the g -strain,³¹ and the spin-spin interactions.²⁰ We do not consider the hyperfine interactions, because for Fe_8 the dominant Fe isotope, ^{56}Fe , has no nuclear spin, and for Mn_{12} there is no resolved hyperfine splitting in the measured EPR spectra. The model and technique in this study are similar to those in Ref. 20. Therefore, we here summarize them only briefly, focusing on what causes the temperature dependence of the line shifts and the linewidths for each source. The temperature dependence of D will be discussed in Sec. IV A.1. In our convention, the energy level $M_s = +10$ is the ground state when the field is applied along the positive z axis, while in Refs. 19,21 the ground state is $M_s = -10$. For clarity, we discuss Fe_8 and Mn_{12} separately.

A. Fe_8

We consider an effective single-spin Hamiltonian which satisfies approximate D_2 symmetry,

$$\mathcal{H}_0 = -DS_z^2 - E(S_x^2 - S_y^2) - g\mu_B H_z S_z , \quad (1)$$

where the uniaxial anisotropy parameter $D = 0.288k_B$, the transverse anisotropy parameter $E = 0.043k_B$,¹⁹ g is the Landé g -factor which is close to 2, and μ_B is the Bohr magneton. Here S_α is the α th component of the spin angular momentum operator, and H_z is the longitudinal static applied magnetic field. We assume that the longitudinal magnetic field is applied along the easy axis (the z axis), and we ignore the small transverse anisotropy terms (E terms) in calculating the linewidths. Thus, the energy level M_s is a good quantum number of the spin operator S_z . According to our convention, the ground state is $M_s = +10$.

Using the density-matrix equation³² with the Hamiltonian, Eq. (1), and an interaction between the spin system and an oscillating transverse field, we calculate the power absorption between the levels M_s and $M_s - 1$ for a fixed value of the uniaxial anisotropy parameter D . In the power absorption, the line-shape function includes a natural linewidth, which is a function of temperature. Next we calculate the average power absorption with a Gaussian distribution in D , where D itself is assumed to be temperature independent. As a consequence, the line broadening due to the D -strain effect becomes weakly temperature dependent because of the temperature dependence of the natural linewidths. To calculate the natural linewidths, we use the strength of the coupling between the spin system and a surrounding phonon heat bath obtained in Ref. 33. For example, for $M_s = +10$, the order of magnitude of the natural linewidths is several to several tens of gauss at temperatures below several tens of kelvin, and the widths increase with decreasing M_s .

The spin-spin interactions are calculated separately with D fixed, and then combined with the D -strain effect to obtain the total linewidths. At low temperatures, all energy levels are not equally populated, and the population of the levels changes with temperature according to the Boltzmann factor. Thus, the local field on a particular molecule caused by surrounding molecules changes with temperature. Therefore, the spin-spin interactions are mainly responsible for the temperature dependence of both the line shifts and the linewidths.^{34,35} To calculate the line shifts and the line broadening due to the spin-spin interactions, we use a multi-spin Hamiltonian which commutes with $\sum_j S_j^z$, where the sum runs over all molecules. Details of the technique can be found in Ref. 35.

$$\mathcal{H}^{\text{tot}} = \sum_i [\mathcal{H}_{0i} + V_i(t)] + \mathcal{H}^{(1)}, \quad (2)$$

$$\mathcal{H}^{(1)} \equiv \mathcal{H}^{\text{dipole}} + \mathcal{H}^{\text{exch}}, \quad (3)$$

$$\mathcal{H}^{\text{dipole}} = \frac{1}{2} \sum_{jk} 'A_{jk} (\vec{S}_j \cdot \vec{S}_k - 3S_j^z S_k^z), \quad A_{jk} \equiv \left(\frac{\mu_0}{4\pi}\right) \frac{(g\mu_B)^2}{2r_{jk}^3} (3\zeta_{jk}^2 - 1), \quad (4)$$

$$\mathcal{H}^{\text{exch}} = \frac{1}{2} \sum_{jk} 'J_{jk} \vec{S}_j \cdot \vec{S}_k, \quad (5)$$

where \mathcal{H}_{0i} is the single-spin Hamiltonian for the i th molecule, the sum \sum_i runs over all molecules, and $V_i(t)$ is the interaction between the i th molecule and the oscillating transverse field. Here $\mathcal{H}^{\text{dipole}}$ is the dipolar interaction between the molecules, and ζ_{jk} are the direction cosines of the vector between molecules j and k (\vec{r}_{jk}) relative to the easy axis (z axis). The sum \sum_{jk}' runs over all molecules, so that any two indices are not the same. $\mathcal{H}^{\text{exch}}$ is the isotropic exchange interaction between the spins of nearest-neighbor molecules. It is reasonable to assume that $\sum_i V_i(t)$ is much smaller than the dipolar and exchange interactions, which again are much smaller than the sum of the single-spin Hamiltonians. Since the field

is swept at constant frequency, the energy levels change with the sweeping field. We neglect slight changes of the energy levels during resonances and use $H_{\text{res}} = (h\nu - D(2M_s - 1))/g\mu_B$, where ν is an EPR frequency, as the field H in the spin Hamiltonian to calculate the energy levels for the particular resonance.

To calculate the ℓ th moment of the resonant field deviation, we formulate the ℓ th moment for a frequency sweep and then convert it to a field sweep. This is justifiable because we neglect the slight energy change caused by the change of the field during a resonance. The probability density function of the EPR frequency ν is given by

$$F_\nu(\nu) = \frac{\sum_n \sum_{n'}^\Delta \{\exp(-\mathcal{E}_n/k_B T) - \exp(-\mathcal{E}_{n'}/k_B T)\} |\langle n | \sum_j S_j^x | n' \rangle|^2}{\sum_n \sum_{n'}^+ \{\exp(-\mathcal{E}_n/k_B T) - \exp(-\mathcal{E}_{n'}/k_B T)\} |\langle n | \sum_j S_j^x | n' \rangle|^2}, \quad (6)$$

where \mathcal{E}_n is the energy eigenvalue of $\sum_j \mathcal{H}_{0j} + \mathcal{H}^{(1)}$, $|n\rangle$ is the corresponding eigenvector, $\sum_{n'}^+$ denotes the sum over all states $|n'\rangle$ such that $\mathcal{E}_{n'} \geq \mathcal{E}_n$, and $\sum_n \sum_{n'}^\Delta$ denotes the sum over all states for which $h\nu \leq \mathcal{E}_{n'} - \mathcal{E}_n \leq h(\nu + d\nu)$. Using Eq. (6), we calculate the ℓ th moment,

$$\langle \nu^\ell \rangle = \frac{\sum_n \sum_{n'}^+ (\mathcal{E}_{n'} - \mathcal{E}_n)^\ell \{\exp(-\mathcal{E}_n/k_B T) - \exp(-\mathcal{E}_{n'}/k_B T)\} |\langle n | \sum_j S_j^x | n' \rangle|^2}{\sum_n \sum_{n'}^+ \{\exp(-\mathcal{E}_n/k_B T) - \exp(-\mathcal{E}_{n'}/k_B T)\} |\langle n | \sum_j S_j^x | n' \rangle|^2}, \ell = 1, 2, \dots, \quad (7)$$

where the temperature dependence of the linewidths is included through the Boltzmann factors, and the eigenvalues of $\mathcal{H}^{(1)}$ can contribute to $(\mathcal{E}_{n'} - \mathcal{E}_n)^\ell$ and/or the Boltzmann factors. Assuming that the dipolar and exchange interactions, $\mathcal{H}^{(1)}$, are much smaller than the thermal energy, we expand the Boltzmann factor into

$$\exp \left[-\frac{\sum_j \mathcal{H}_{0j} + \mathcal{H}^{(1)}}{k_B T} \right] = \exp \left(-\frac{\sum_j \mathcal{H}_{0j}}{k_B T} \right) \left[1 - \frac{\mathcal{H}^{(1)}}{k_B T} + \dots \right] \quad (8)$$

and consider only the first term on the right-hand side. In Ref. 36, the Boltzmann factor was not included since the temperature of interest was quite high, so that all energy levels were equally populated. In our calculations, we use a mean-field approximation, so that the sums of A_{jk} and J_{jk} [Eqs. (4) and (5)] can be separated from the spin operators.

To compare with the measured *line shifts*, we calculate perturbatively the first moment, $\langle H - H_{\text{res}} \rangle$, where H_{res} is the resonant field without the spin-spin interactions, and subtract from it the first moment at a reference temperature, 30 K. This reference temperature was chosen because at higher temperatures additional line shifts can be expected from the temperature dependence of D . The calculated line shifts to zero order in $\mathcal{H}^{(1)}/k_B T$ contain the exchange coupling constant J and the effective dipole field $\Delta \equiv \sum_{j \neq k} A_{jk}/N$ (N is the number of molecules in the sample and the summation runs over all molecules) as variable parameters. This zero-order result in $\mathcal{H}^{(1)}/k_B T$ depends on J and Δ through the terms $(\mathcal{E}_{n'} - \mathcal{E}_n)$ in Eq. (7). Since Δ depends on the sample shape due to the field-induced net magnetization, Ewald's method³⁷ is not sufficient to estimate its value in our case.

To compare with the measured *linewidths*, we need to calculate the second central moment, $\langle (H - \langle H \rangle)^2 \rangle$, which is equivalent to $\langle (H - H_{\text{res}})^2 \rangle - (\langle H - H_{\text{res}} \rangle)^2$, where $\langle (H - H_{\text{res}})^2 \rangle$ and $(\langle H - H_{\text{res}} \rangle)^2$ are calculated perturbatively to zero order in $\mathcal{H}^{(1)}/k_B T$.³⁵ The square root of the second central moment is proportional to the broadening due to the spin-spin interactions. The quantity $\langle (H - H_{\text{res}})^2 \rangle$ includes the following six terms, $\sum'_{ij} J_{ij}^2$, $\sum'_{ij} J_{ij} A_{ij}$, $\sum'_{ij} A_{ij}^2$, $\sum'_{ijk} J_{ij} J_{jk}$, $\sum'_{ijk} J_{ij} A_{jk}$, and $\sum'_{ijk} A_{ij} A_{jk}$. The quantity $(\langle H - H_{\text{res}} \rangle)^2$ includes three

terms, $(\sum'_{ij} J_{ij})^2/N$, $(\sum'_{ij} J_{ij})(\sum'_{ij} A_{ij})/N$, and $(\sum'_{ij} A_{ij})^2/N$. Here \sum'_{ij} and \sum'_{ijk} run over all molecules with the constraint that any two indices in the summations must not be the same, and J_{ij} and J_{jk} are nonzero for nearest-neighbor molecules only. The coefficients of the last three terms (the summations over three indices i , j , and k) in $\langle (H - H_{\text{res}})^2 \rangle$ are the same as those of the three terms in $\langle (H - H_{\text{res}}) \rangle^2$. To simplify the second central moment, we use the identities

$$\frac{1}{N} \left(\sum_{ij} ' J_{ij} \right)^2 = \sum_{ij} ' J_{ij}^2 + \sum_{ijk} ' J_{ij} J_{jk} , \quad (9)$$

$$\frac{1}{N} \left(\sum_{ij} ' J_{ij} \right) \left(\sum_{ij} ' A_{ij} \right) = \sum_{ij} ' J_{ij} A_{ij} + \sum_{ijk} ' J_{ij} A_{jk} , \quad (10)$$

$$\frac{1}{N} \left(\sum_{ij} ' A_{ij} \right)^2 = \sum_{ij} ' A_{ij}^2 + \sum_{ijk} ' A_{ij} A_{jk} . \quad (11)$$

Summations over four different indices do not appear in Eq. (11) because $\sum'_{ij} A_{ij} = N \sum_{j \neq 1} A_{1j}$ by translational invariance. We thus have only three undetermined terms, $\sum'_{ij} J_{ij}^2$, $\sum'_{ij} A_{ij}^2$, and $\sum'_{ij} J_{ij} A_{ij}$ in the calculated second central moment. The exchange coupling constant J could be determined from the line-shift analysis. The remaining two terms, $\sum'_{ij} A_{ij}^2$ and $\sum'_{ij} J_{ij} A_{ij}$, can, in principle, be calculated from the exact geometry of the system. However, in our study, we take the two terms as variable parameters, and compare their optimum values with the calculated values. Physical justification for this is discussed in Sec. IV.A.2.

We fix the EPR frequency at $\nu = 116.9$ GHz and vary the temperature from 4 K to 35 K for the linewidth analysis (2 K to 30 K for the line-shift analysis). We do not analyze the experimental data above 35 K because at higher temperatures excited states (effective spin $S < 10$) might play a role. Only good-quality (high signal-to-noise ratio) experimental data were selected. For the line-shift analysis, the exchange constant J and effective dipole field Δ are varied, while for the linewidth analysis, $\Gamma \equiv \sum'_{ij} A_{ij}^2/N$, $\Lambda \equiv \sum'_{ij} J_{ij} A_{ij}/N$, and the standard deviation of D are varied within experimentally acceptable ranges in order to fit the experimental data.

B. Mn₁₂

For Mn₁₂ we consider an effective single-spin Hamiltonian which satisfies tetragonal symmetry,

$$\mathcal{H}_0 = -DS_z^2 - CS_z^4 - g\mu_B H_z S_z \quad (12)$$

with $D=0.55k_B$, $C=1.17 \times 10^{-3}k_B$, and $g=1.94$.³ Here we consider the case in which the applied field is along the easy axis (the z axis), and we neglect the small transverse fourth-order anisotropy term, $S_x^4 + S_y^4$.

The technique is the same as for Fe₈, except for the following: (i) The g -strain effect provides a weak temperature dependence to the linewidths, caused by the temperature dependence of the natural linewidths. (ii) The resonant field without the spin-spin interactions is modified to

$$H_{\text{res}} \equiv \frac{h\nu - D(2M_s - 1) + C(4M_s^3 - 6M_s^2 + 4M_s - 1)}{g\mu_B} . \quad (13)$$

(iii) To calculate the natural linewidths, we use the strength of the coupling between the spin system and a surrounding phonon heat bath from Ref. 38. (iv) The easy anisotropy axis is along the long side of the needle-shaped sample. (v) For Mn_{12} the measured line shifts are negligible compared to the measured linewidths, so that we do not have to consider the exchange interaction and the effective dipole field ($J = 0$ and $\Delta = 0$, so $\Gamma = 0$). Thus, the second *central* moment $\langle (H - \langle H \rangle)^2 \rangle$, which is proportional to the measured linewidths, is identical to the second moment $\langle (H - H_{\text{res}})^2 \rangle$.

To compare with the experimental data, the frequency is fixed at $\nu = 189.123$ GHz, and the temperature is varied from 10 K to 40 K. Our analysis ends at 40 K because at higher temperatures excited states (effective spin $S < 10$) might play a role.^{39–41} Only EPR spectra of good quality were selected, and Γ and the standard deviations of D and g were varied within acceptable ranges in order to fit the experimental data.

IV. RESULTS AND DISCUSSION

We show that the spin-spin interactions (dipolar and/or exchange interactions) alone determine the trend of the temperature dependence of the line shifts and the linewidths. From the line-shift analysis, we can estimate the orders of magnitude of the exchange interaction and the effective dipole field and obtain their signs. Using this information, we can also explain quantitatively the linewidths, including the D -strain and/or the g -strain effects which give rise to a strong M_s dependence but weak temperature dependence of the linewidths. The spin-spin interactions contribute more to the linewidths for Fe_8 than for Mn_{12} , mainly because the D -strain effect is dominant over the spin-spin interactions for Mn_{12} , while it is comparable with the spin-spin interactions for Fe_8 . This explains the different temperature behavior of the linewidths for Fe_8 and Mn_{12} . The set of parameter values which best explains the experimental data has some systematic theoretical uncertainties, which are difficult to calculate exactly.

A. Fe_8

1. line shifts

It is known that the value of the uniaxial anisotropy parameter D may vary smoothly with temperature.⁴² To gauge the importance of this effect, we first assume that D has a temperature dependence such as Fig. 1(a). Then the line shift, $\langle H \rangle(T) - \langle H \rangle(T=30 \text{ K})$, becomes monotonically temperature dependent, as shown in Fig. 1(b). Comparing Fig. 1(b) with the experimental data in Fig. 2(a), we see that the monotonic temperature dependence of D cannot by itself explain the complicated temperature dependence of the measured line shifts. It could presumably contribute together with other factors which will be described below. However, we hereafter take D as a temperature independent parameter, for the sake of simplicity and because the exact temperature behavior is not yet known. We also note that the distribution in D does not change the line positions.

Next, we consider the effect of the spin-spin interactions between molecules on the measured line shifts. If we first ignore the exchange interaction and consider the dipolar interaction only for a spherical sample with dipoles distributed on a simple cubic lattice, then the effective dipole field Δ vanishes, so that there is no line shift to zero order in $\mathcal{H}^{(1)}/k_B T$. Higher-order corrections [the second term in Eq. (8)] provide a much smaller and qualitatively different temperature dependence from that seen in the measurements. [Compare Fig. 3(a) with Fig. 2(a).] If we include a non-zero effective dipole field Δ only in the zero-order calculation, then a negative effective dipole field moves the line shifts for all the transitions down below zero [Fig. 3(b)]. On the other hand, if we include an exchange interaction only in the zero-order calculation, then a ferromagnetic exchange interaction (negative J) moves the line shifts up above zero for all transitions except $M_s = +10$ [Fig. 3(c)]. In both cases, the calculated line shifts behave very differently from the measured shifts [Fig. 2(a)]. Therefore, we need to include both the effective dipole field and the exchange interaction in order to explain the measured line shifts. An inter-molecular exchange interaction was recently observed for the different types of single-molecule magnets, Mn_4 and Mn_4 dimer.⁴³ Since the effective dipole field Δ depends on the sample shape due to the field-induced net magnetization, we do not use the Ewald's method³⁷ to estimate Δ and thus leave it as a fitting parameter. For the exchange interaction, we assume that the coupling constant J_{ij} is isotropic along the a , b , and c directions of the triclinic unit cell (although in experimental samples the exchange interactions are highly anisotropic), so that the coordination number is 6. The optimum values of Δ and J are $\Delta_{\text{opt}} \approx -20$ gauss and $J_{\text{opt}} \approx -7$ gauss (~ 1 mK) respectively. With these optimum values, the calculated line shifts [Fig. 2(b)] reproduce well the trends of the temperature dependence of the experimental data [Fig. 2(a)]. Figure 2(c) shows a direct comparison between theory and experiment for a few transitions.

The negative sign of the effective dipole field ($\Delta < 0$) indicates that dipoles are anti-ferromagnetically coupled. This result seems to be in conflict with the prediction that the dipolar Ising spin system with the same structure as Fe_8 is ferromagnetically ordered.^{44,45} However, as pointed out in Ref. 45, the energy difference between the ferromagnetic and antiferromagnetic states is so small that any neglected effects may shift the ground state to an antiferromagnetic state. The negative sign of the exchange coupling constant ($J < 0$) corresponds to ferromagnetical coupling between the effective spins of the molecules. Thus, if there exists any ordering for Fe_8 , then the ordering temperature should be estimated by considering both the exchange and dipolar interactions. The two interactions compete with each other, thereby reducing the possible ordering temperature to a lower value than the ordering temperature with only one of the two interactions considered.

Finally, we show the calculated line shifts with several other parameter values that are different from the optimum ones. If the effective dipole field and the exchange interaction both change signs, then the calculated line shift also changes its sign. If the sign of Δ is opposite to the sign of J , then the magnitude of the calculated line shift for $M_s = +10$ is much smaller than those for the other transitions, which does not agree with the experimental data. [Compare Fig. 3(d) with Fig. 2(a).] Figure 3(e) shows the calculated line shifts with $J < J_{\text{opt}}$ and $\Delta = \Delta_{\text{opt}}$. Figure 3(f) shows the calculated line shifts with $J = J_{\text{opt}}$ and $\Delta < \Delta_{\text{opt}}$. All three figures [Figs. 3(d)-(f)] are significantly different from Fig. 2(b) with the optimized values.

2. linewidths

For Fe_8 the distribution in D and the spin-spin interactions contribute approximately equally to the inhomogeneous line broadening. Figure 4 shows the calculated line broadening due to the D -strain effect only as a function of temperature at $\nu = 116.9$ GHz. Here the standard deviation of the Gaussian distribution in D , σ_D , is approximately $0.0064D$. The line broadening caused by the D -strain only becomes temperature dependent, because the natural linewidths depend on temperature. The distribution in D makes each molecule subject to a slightly different resonant field. A measured line shape is a sum of many Lorentzian line shapes with a natural linewidth and different resonant fields. We can calculate the variance of the resonant field, $\sigma_D(2M_s - 1)/g\mu_B$, due to the distribution in D from the expression for H_{res} . If the natural linewidths are comparable with the variance of the resonant field, then the effect of temperature is significant. If the natural linewidths are much smaller than the variance, then the effect of temperature is negligible. The natural linewidth at 10 K (35 K) varies from 7 G (29 G) to 79 G (235 G) as M_s changes from +10 to +3, using the parameter values in Ref. 33. The variance of the resonant field, $\sigma_D(2M_s - 1)/g\mu_B$, varies from 260 G to 70 G as M_s is varied from +10 to +3 with $\sigma_D = 0.0064D$. Thus, we find that for small M_s the natural linewidths are comparable with the variance, while for large M_s the natural linewidths are much smaller than the variance. Therefore, for small M_s the calculated linewidths show a substantial temperature dependence, while for large M_s there is only a very weak temperature dependence (see Fig. 4).

In Fig. 5 the calculated line broadening caused solely by the spin-spin interactions at fixed D is shown vs temperature at $\nu = 116.9$ GHz. Here we use the exchange constant, $J = -7$ gauss, which was estimated in the measured line shifts (Sec. IV A.1), $\Gamma \equiv \sum_{ij} A_{ij}^2/N = 86$ gauss 2 , and $\Lambda \equiv \sum_{ij} J_{ij}A_{ij}/N = -156$ gauss 2 . For the ground state $M_s = +10$, the linewidths decrease with increasing temperature in the whole examined temperature range. For $M_s = +9, +8$, and $+7$, the widths first increase sharply with temperature at low temperatures, and then decrease slowly with temperature at high temperatures. For $M_s = +6, +5, +4$, and $+3$, the widths increase with increasing temperature in the whole examined temperature range. As the temperature increases, the M_s dependence of the line broadening due to the spin-spin interactions decreases. This trend was also seen in the experimental linewidths (shown as symbols in Fig. 6), confirming that the spin-spin interactions are essential to understanding the temperature dependence of the linewidths.

The trends of the temperature dependence can be qualitatively understood through the relative magnitude difference of the thermal energy and the Zeeman energy splitting between the states $M_s = +10$ and $M_s = -10$. If the Zeeman energy splitting is much larger than the thermal energy (this occurs at low temperatures), then the system is polarized. Thus, higher temperature provides larger populations in higher energy levels within the same potential well where the ground state is located. This leads to an increase in the randomness of the spin orientation so that linewidths become larger with increasing temperature. If the Zeeman energy splitting is much smaller than the thermal energy (this occurs at high temperatures), then some energy levels in *both* potential wells are populated. In this case, thermal fluctuations increase rapidly with increasing temperature, so that the duration time of the local magnetic field due to neighboring molecules becomes shorter than the spin-spin relaxation time T_2 (the inverse of the natural linewidths). Eventually, at very

high temperatures the local field is averaged out. Therefore, the linewidths decrease with increasing temperature, which usually occurs in paramagnetic materials with very small or zero single-ion anisotropy.⁴⁶ (This effect is called motional narrowing.³⁴) Therefore, the “crossover” temperature where the maximum of the linewidth occurs must be proportional to the Zeeman energy splitting between $M_s = +10$ and $M_s = -10$, which is $2g\mu_B H_{\text{res}} \cdot 10$. For example, for the transition $M_s = +10 \rightarrow +9$ at $\nu = 116.9$ GHz, the resonant field is less than 0.1 T, so the Zeeman splitting is about $2k_B$. Consequently, its crossover temperature is below the examined temperature range. The crossover temperature increases with decreasing M_s because the resonances are observed at increasing fields for decreasing M_s . For the transitions $M_s = +9 \rightarrow +8$, $+8 \rightarrow +7$, and $+7 \rightarrow +6$, the crossover temperatures are within the examined temperature range. (See the inset in Fig. 6 of Ref. 21.) For $M_s = +6, +5, +4$, and $+3$, the crossover temperatures are above the studied temperature range.

Figure 6 shows the experimental data (symbols), and our calculated linewidths (curves), including both the D -strain effect and the spin-spin interactions with $\sigma_D \approx 0.0064D$, $J = -7$ gauss, $\Gamma = 86$ gauss², and $\Lambda = -156$ gauss². As shown in Fig. 6, our calculated linewidths agree well with the experimental data, except in the low-temperature range for large M_s transitions ($M_s = +10, +9, +8$). The experimental linewidths for $M_s = +10$ show $1/T$ dependence in the whole examined temperature range.⁴⁷ For $M_s = +10, +9$, and $+8$, the calculated linewidths are appreciably smaller than the experimental linewidths below 10 K. As a possible explanation for this discrepancy, we speculate that at low temperatures and large M_s , (i) our assumption, $\mathcal{H}^{(1)}/k_B T \ll 1$, may break down, and/or (ii) there might be other linewidth contributions that we have neglected, which should be included along with the dipolar and exchange interactions. In principle, when $\mathcal{H}^{(1)}/k_B T$ is not much smaller than unity, a first-order calculation in $\mathcal{H}^{(1)}/k_B T$ produces corrections of $\mathcal{O}(1/k_B T)$. But its implementation is quite complicated, and a first-order calculation may anyway not be sufficient to explain fully the measured linewidths.

Introducing the concept of the crossover temperature to explain the temperature dependence of the widths seems to be successful for $\nu = 116.9$ GHz. However, recent EPR experiments (Fig. 8 in Ref. 21) showed that even when the frequency increased to $\nu = 145.9$ GHz such that the resonant field for the ground state transition ($M_s = 10$) is approximately 1 tesla, the linewidths for this transition still increased with *decreasing* temperatures down to 2 K. This cannot be explained using the reasoning given above, because the crossover temperature for the transition is approximately 15 K, so that the linewidths should decrease with decreasing temperature below about 15 K. At present, we do not fully understand the broadening of this ground-state transition. (At $\nu = 145.9$ GHz, for other transitions than the ground-state transition, the temperature dependence of the linewidths can be understood using the concept of the crossover temperature.)

Consideration of exchange interaction in the linewidths slightly reduces σ_D (from 0.0076D to 0.0064D) and the dipolar interaction (from $\Gamma = 103$ gauss² to $\Gamma = 86$ gauss²). However, the quality of the linewidth fit including exchange interaction is comparable to that without exchange interaction since the exchange coupling constant is very small compared with the linewidths.³⁴ The two fitting parameters, $\Gamma = 86$ gauss², and $\Lambda = -156$ gauss², can be calculated using the exact geometry of the system. The calculated values are $\Gamma_{\text{cal}} = 500$ gauss² and $\Lambda_{\text{cal}} = -137$ gauss², when the easy axis is 9° off from the a axis toward the positive b axis, and 7° off from the ab plane.⁴⁸ The optimum value of Λ is quite close to

Λ_{cal} , in contrast with Γ . Possible reasons that the optimum value of Γ is much smaller than Γ_{cal} are as follows: (i) In our calculation, we considered each molecule to be a point dipole. If we consider the atomic positions of the eight Fe ions in each molecule and calculate the dipolar interaction between Fe ions in different molecules, then the sum of the squared dipolar interaction, Γ , can be significantly reduced. (ii) Recent NMR experiments for the single-molecule magnet Mn_{12} showed some spin-density leakage onto the ligands.^{26–28} This indicates indirectly that for Fe_8 the spin density in a single molecule may not be confined only on the core, which would thus reduce the magnetic moments of the eight Fe ions.

B. Mn_{12}

For Mn_{12} , it is found that the measured line shifts are considerably smaller than the measured linewidths. Thus, hereafter, the small line shifts are ignored in the analysis of the linewidths, so the exchange interaction and the effective dipole field Δ need not to be considered for Mn_{12} . The sources of the line broadening are then D -strain, g -strain, and the dipolar interaction.

Line broadening caused by the D -strain and g -strain effects for Mn_{12} is found to have a weak temperature dependence (not shown), which is similar to the line broadening due to the D -strain effect for Fe_8 . The contribution of the dipolar interaction to the linewidths is shown vs temperature in Fig. 7. Here $\Gamma \equiv \sum_{ij} A_{ij}^2 / N = 203 \text{ gauss}^2$. The dipolar broadening increases with increasing temperature for $M_s = +6, +5, +4, +3$, and $+2$. We do not see the regime where the dipolar broadening decreases with increasing temperature, because the crossover temperature for $M_s = +6$, about 32 K (the resonant field is about 1.6 T), is close to the highest temperature analyzed (40 K). Unlike Fe_8 , the M_s dependence of the dipolar broadening does not decrease with increasing temperature (the curves are almost parallel). This is also observed in the experimental data (shown as symbols in Fig. 8).

We combine the three effects (D -strain, g -strain, and dipolar interactions) to find that the calculated linewidths agree well with the measured linewidths with $\sigma_D \approx 0.018D$, $\sigma_g \approx 0.002g$, and $\Gamma = 203 \text{ gauss}^2$, as shown in Fig. 8. Here the standard deviation of g is quite small, so that we cannot rule out the possibility of $\sigma_g = 0$. Note that σ_D and σ_g vary from sample-to-sample. The optimum parameter values found here are different from those estimated in Ref. 20, because the examined Mn_{12} sample was different. The calculated value for Γ , with the exact geometry of Mn_{12} from Ref. 1 (when a molecule is considered as a point dipole), is $\Gamma_{\text{cal}} = 397 \text{ gauss}^2$; this is, again, quite a bit higher than the optimum value for Γ , probably for the same reasons as for Fe_8 . Overall, the temperature dependence of the linewidths for Mn_{12} is weaker than for Fe_8 , because the distribution in D for Mn_{12} is roughly three times as wide as for Fe_8 , and the dipolar broadening for Fe_8 is comparable to that for Mn_{12} . Thus, the distribution in D conceals the significant temperature dependence of the dipolar broadening for Mn_{12} .

As a consistency check, we also used the same values of the three parameters ($\sigma_D \approx 0.018D$, $\sigma_g \approx 0.002g$, and $\Gamma = 203 \text{ gauss}^2$) to analyze the measured linewidths²¹ as functions of the energy level M_s for several frequencies ($\nu = 127.8, 148.5, 169, 181.8$, and 189.1 GHz) at a fixed temperature ($T=20 \text{ K}$). Our calculated linewidths are in good agreement with the experimental data as shown in Fig. 9. Due to a dominant contribution of the distribution in D to the linewidths, the linewidths do not depend much on the resonance frequency.

V. CONCLUSION

We have investigated how the EPR line shifts and linewidths vary with temperature for different energy levels M_s with the applied field along the easy axis for the single-molecule magnets Fe_8 and Mn_{12} . Our calculations consider the spin-spin interactions between molecules and distributions in D and g . We have found that the distributions in D and g provide a weak temperature dependence to the linewidths, and that the spin-spin interactions (exchange and dipolar interactions) dominate the temperature dependence of the line shifts and the linewidths. For Fe_8 , the line-shift analysis (Figs. 2 and 3) provides possible evidence of an exchange interaction between molecules, and determines the sign and order of magnitude of the exchange interaction. The competition of the suggested exchange interaction with the dipolar interaction would tend to lower a possible magnetic ordering temperature. A small exchange interaction does not affect the linewidth analysis significantly because the exchange coupling constant is much smaller than the typical linewidths. Table I summarizes the optimized values of the parameters used in our analysis. Because of the much broader distribution in D for Mn_{12} , the linewidths for Fe_8 show a stronger temperature dependence than those for Mn_{12} . This conclusion also corroborates our assumption that D is distributed for both materials,²⁰ although the microscopic origin of this spread is not yet well understood.^{23,24}

Acknowledgments

This work was funded by NSF Grant Nos. DMR-9871455, DMR-0120310, DMR-0103290, and DMR-0196430, Research Corporation (S.H.), and by Florida State University through the School of Computational Science and Information Technology and the Center for Materials Research and Technology.

REFERENCES

- * Electronic address: park@csit.fsu.edu
- † Electronic address: man40@ra.msstate.edu
- ‡ Electronic address: dalal@chem.fsu.edu
- § Electronic address: hill@phys.ufl.edu
- || Electronic address: rikvold@csit.fsu.edu
- ¹ T. Lis, *Acta Crystallogr. B* **36**, 2042 (1980).
- ² K. Wieghart, K. Pohl, I. Jibril, and G. Huttner, *Angew. Chem. Int. Ed. Engl.* **23**, 77 (1984).
- ³ A. L. Barra, D. Gatteschi, and R. Sessoli, *Phys. Rev. B* **56**, 8192 (1997).
- ⁴ S. Hill, J. A. A. J. Perenboom, N. S. Dalal, T. Hathaway, T. Stalcup, and J. S. Brooks, *Phys. Rev. Lett.* **80**, 2453 (1998).
- ⁵ J. A. A. J. Perenboom, J. S. Brooks, S. Hill, T. Hathaway, and N. S. Dalal, *Phys. Rev. B* **58**, 330 (1998).
- ⁶ I. Mirebeau, M. Hennion, H. Casalta, H. Andres, H. U. Güdel, A. V. Irodova, and A. Caneschi, *Phys. Rev. Lett.* **83**, 628 (1999).
- ⁷ R. Caciuffo, G. Amoretti, A. Murani, R. Sessoli, A. Caneschi, and D. Gatteschi, *Phys. Rev. Lett.* **81**, 4744 (1998).
- ⁸ A. Garg, *Europhys. Lett.* **22**, 205 (1993).
- ⁹ *Quantum Tunneling of Magnetization – QTM '94*, Vol. 301 of *NATO Advanced Study Institute, Series E: Applied Sciences*, edited by L. Gunther and B. Barbara (Kluwer, Dordrecht, 1995).
- ¹⁰ J. Villain, F. Hartman-Boutron, R. Sessoli, and A. Rettori, *Europhys. Lett.* **27**, 159 (1994).
- ¹¹ E. M. Chudnovsky and J. Tejada, *Macroscopic Quantum Tunneling of the Magnetic Moment*, Cambridge Studies in Magnetism, Vol. 4 (Cambridge University Press, Cambridge, 1998) and references therein.
- ¹² N. V. Prokof'ev and P. C. E. Stamp, *Phys. Rev. Lett.* **80**, 5794 (1998).
- ¹³ T. Ohm, C. Sangregorio, and C. Paulsen, *Eur. Phys. J. B* **6**, 195 (1998).
- ¹⁴ A. Cuccoli, A. Fort, A. Rettori, E. Adam, and J. Villain, *Eur. Phys. J. B* **12**, 39 (1999).
- ¹⁵ W. Wernsdorfer, T. Ohm, C. Sangregorio, R. Sessoli, D. Mailly, and C. Paulsen, *Phys. Rev. Lett.* **82**, 3903 (1999).
- ¹⁶ S. Miyashita and K. Saito, *J. Phys. Soc. Jpn.* **70**, 3385 (2001).
- ¹⁷ J. Liu, B. Wu, L. Fu, R. B. Diener, and Q. Niu, cond-mat/0105497 (unpublished).
- ¹⁸ R. Blinc, P. Cevic, D. Arcon, N. S. Dalal, and R. M. Achey, *Phys. Rev. B* **63**, 212401 (2001).
- ¹⁹ S. Maccagnano, R. Achey, E. Negusse, A. Lussier, M. M. Mola, S. Hill, and N. S. Dalal, *Polyhedron*, **20**, 1441 (2001).
- ²⁰ K. Park, M. A. Novotny, N. S. Dalal, S. Hill, and P. A. Rikvold, *Phys. Rev. B* **65** 014426 (2002).
- ²¹ S. Hill, S. Maccagnano, K. Park, R. M. Achey, J. M. North, and N. S. Dalal, accepted for publication in *Phys. Rev. B*; cond-mat/0112172 (unpublished).
- ²² B. Parks, J. Loomis, E. Rumberger, D. Hendrickson, and G. Christou, *Phys. Rev. B* **64**, 184426 (2001).
- ²³ E. M. Chudnovsky and D. A. Garanin, *Phys. Rev. Lett.* **87**, 187203 (2001); *Phys. Rev. B* **65**, 094423 (2002).

²⁴ A. Cornia, R. Sessoli, L. Sorace, D. Gatteschi, A. L. Barra, and C. Daiguebonne, cond-mat/0112112 (unpublished).

²⁵ A. Mukhin B. Gorshunov, M. Dressel, C. Sangregorio, and D. Gatteschi, Phys. Rev. B **63**, 214411 (2001).

²⁶ R. M. Achey, P. L. Kuhns, W. G. Moulton, and N. S. Dalal, Phys. Rev. B , **64**, 064420 (2001).

²⁷ R. M. Achey, P. L. Kuhns, A. Reyes, and N. S. Dalal, Polyhedron, **20**, 1745 (2001).

²⁸ R. M. Achey, P. L. Kuhns, A. P. Reyes, and N. S. Dalal, Sol. St. Commun. **121**, 107 (2002).

²⁹ M. Mola, S. Hill, M. Gross, and P. Goy, Rev. Sci. Instrum. **71**, 186 (2000); S. Hill, N. S. Dalal, and J. S. Brooks, Appl. Magn. Reson. **16**, 237 (1999).

³⁰ N. S. Dalal, Advan. Magn. Reson. **10**, 119 (1982).

³¹ J. R. Pilbrow, *Transition Ion Electron Paramagnetic Resonance* (Clarendon, Oxford, 1990).

³² K. Blum, *Density Matrix Theory and Applications*, 2nd edition (Plenum, New York, 1996).

³³ M. N. Leuenberger and D. Loss, Phys. Rev. B **61**, 12200 (2000).

³⁴ A. Abragam and B. Bleaney, *Electron Paramagnetic Resonance of Transition Ions* (Clarendon, Oxford, 1970).

³⁵ M. McMillan and W. Opechowski, Can. J. Phys. **38**, 1168 (1960); *ibid.* **39**, 1369 (1961).

³⁶ J. H. Van Vleck, Phys. Rev. **74**, 1168 (1948).

³⁷ P. P. Ewald, Ann. Phys. (Leipzig) **64**, 253 (1921).

³⁸ M. N. Leuenberger and D. Loss, Phys. Rev. B **61**, 1286 (2000).

³⁹ M. Hennion, L. Pardi, I. Mirebeau, E. Suard, R. Sessoli, and D. Gatteschi, Phys. Rev. B **56**, 8819 (1997).

⁴⁰ A. M. Gomes, M. A. Novak, R. Sessoli, A. Caneschi, and D. Gatteschi, Phys. Rev. B **57**, 5021 (1998).

⁴¹ B. Barbara, L. Thomas, F. Lioni, A. Sulpice, and A. Caneschi, J. Magn. Magn. Mater. **177**, 1324 (1998).

⁴² R. P. Penrose and K. W. H. Stevens, Proc. Phys. Soc. **63**, 29 (1950).

⁴³ W. Wernsdorfer, N. Aliaga-Alcalde, D. N. Hendrickson, and G. Christou, Nature **416**, 406 (2002).

⁴⁴ J. Fernández and J. J. Alonso, Phys. Rev. B **62**, 53 (2000); to appear in Phys. Rev. B.

⁴⁵ X. Martínez-Hidalgo, E. M. Chudnovsky, and A. Aharony, Europhys. Lett. **55**, 273 (2001).

⁴⁶ B. E. Larson and H. Ehrenreich, Phys. Rev. B **39**, 1747 (1989).

⁴⁷ S. Hill, S. Maccagnano, N. S. Dalal, R. Achey and K. Park: “D-strain, g-strain, and dipolar interactions in the Fe₈ and Mn₁₂ single-molecule magnets: an EPR lineshape analysis”, submitted to *Physical Phenomena in High Magnetic Fields - IV*, edited by G. Boebinger, L. P. Gor’kov, A. Lacerda and J. R. Schrieffer (World Scientific, Singapore, in press).

⁴⁸ W. Wernsdorfer, private communication.

FIGURES

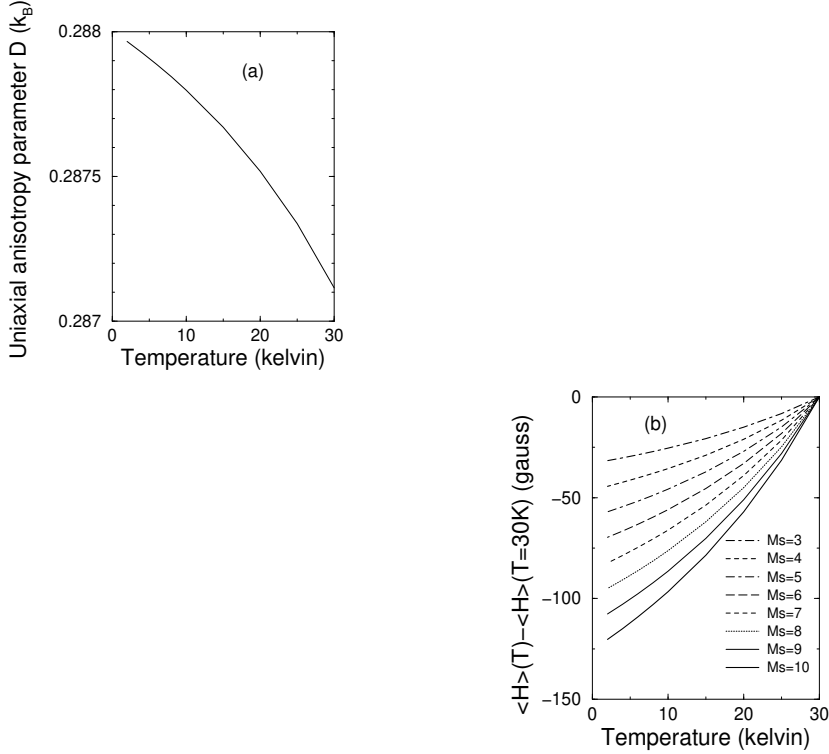
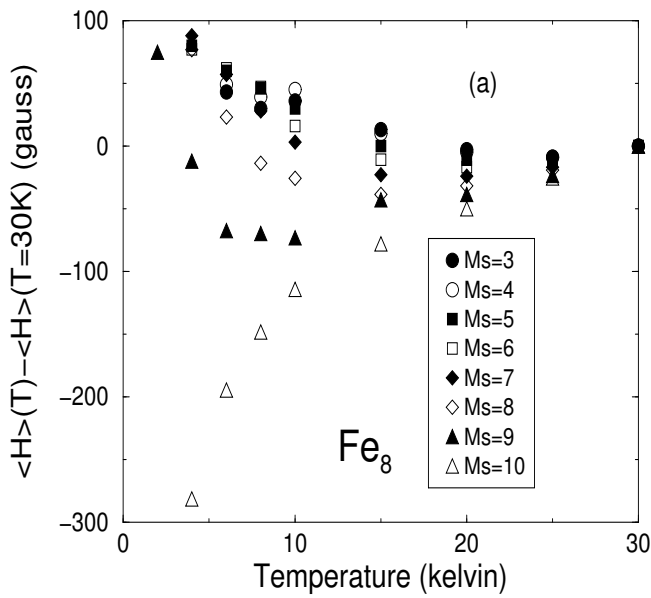


FIG. 1. (a) Hypothetical smooth temperature dependence of the uniaxial anisotropy parameter D for Fe_8 . The functional form used here is $D(T) = -0.710665 + \exp\{-1/[10(50 - T) + 250]\}$. (b) The resulting calculated line shifts (the peak position at a given temperature minus the position at $T = 30$ K) due to this temperature dependence of D , shown vs temperature at $\nu = 116.9$ GHz.



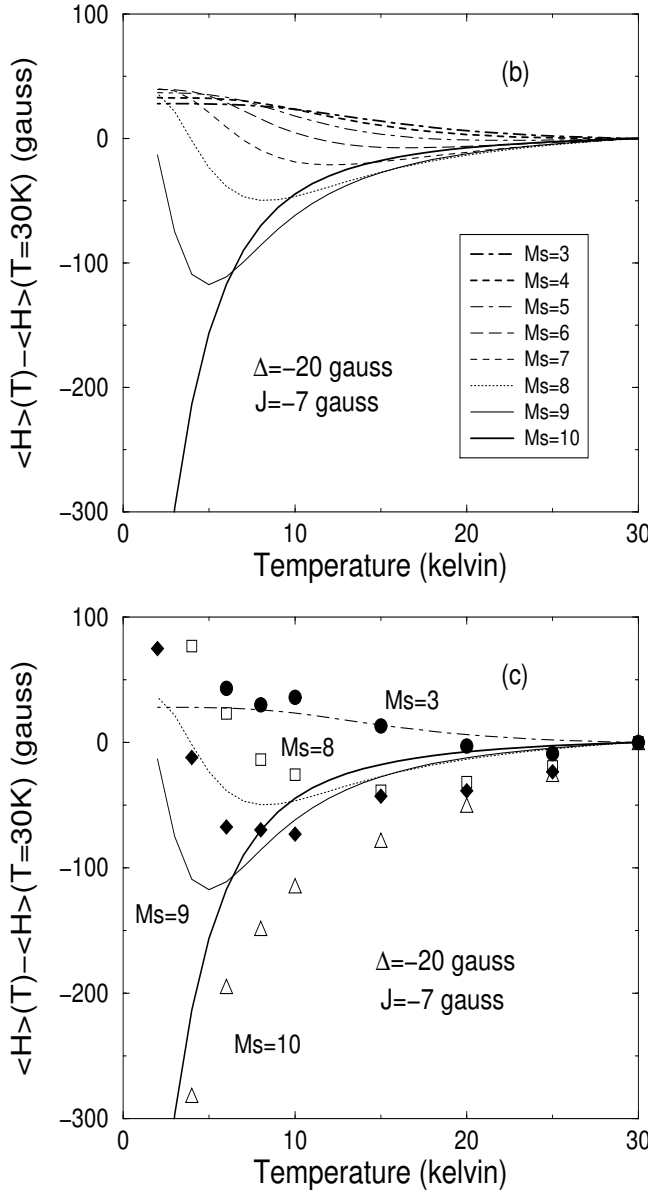
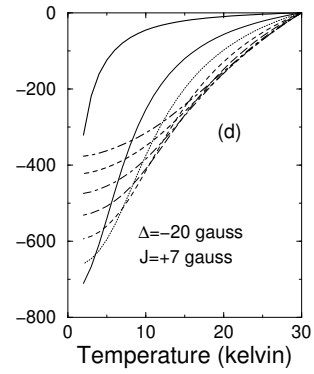
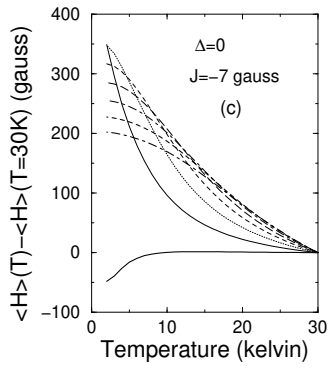
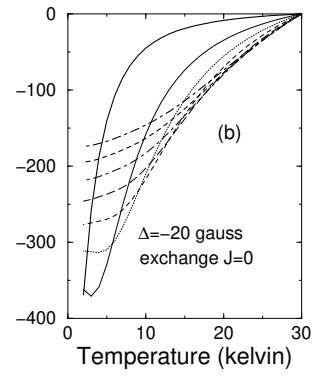
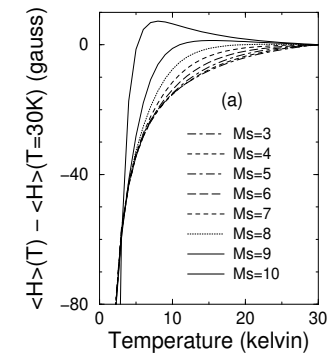


FIG. 2. (a) Measured line shifts vs temperature at $\nu = 116.9$ GHz for Fe₈. (b) Calculated line shifts vs temperature at $\nu = 116.9$ GHz for Fe₈. Here the calculation is performed to zero order in $\mathcal{H}^{(1)}/k_B T$. We use the effective dipole field $\Delta \equiv \sum_{ij} A_{ij}/N = -20$ gauss and the exchange coupling constant $J = -7$ gauss. (c) Measured line shifts (symbols in (a)), superimposed on calculated line shifts (curves in (b)), for several transitions for comparison.



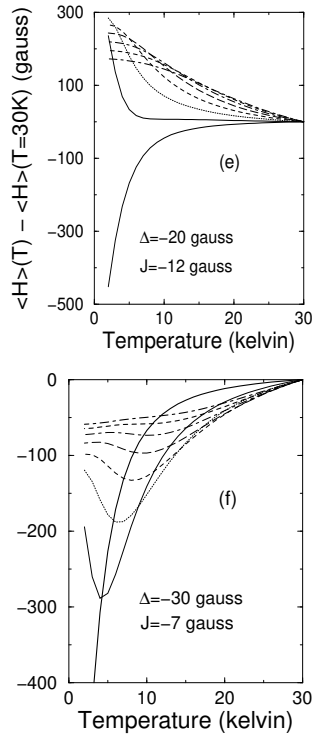


FIG. 3. Calculated line shifts vs temperature at $\nu = 116.9$ GHz for Fe_8 , with (a) only the dipolar interaction for a spherical sample in higher-order calculations ($J = 0$, $\Delta \equiv \sum'_{ij} A_{ij}/N = 0$, and $\Gamma \equiv \sum'_{ij} A_{ij}^2/N \neq 0$) (b) only the effective dipole field, $\Delta = -20$ gauss, (c) only the exchange coupling constant, $J = -7$ gauss, (d) $\Delta = -20$ gauss < 0 and $J = +7$ gauss > 0 , (e) $\Delta = -20$ gauss and $J = -12$ gauss, and (f) $\Delta = -30$ gauss and $J = -7$ gauss.

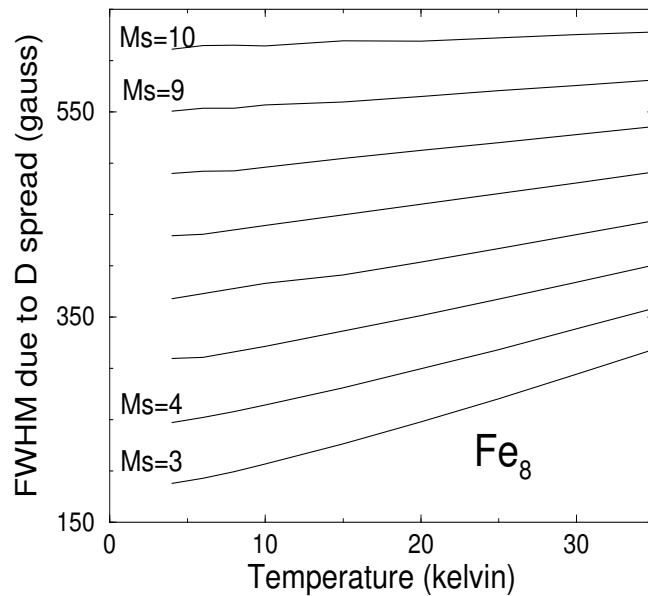


FIG. 4. Calculated full width at half maximum (FWHM) caused by the Gaussian distribution in the uniaxial anisotropy parameter D only, shown vs temperature from 4 K to 35 K at $\nu = 116.9$ GHz for Fe_8 . $M_s = 10$ indicates the transition from the energy level $M_s = 10$ to $M_s = 9$, etc. The standard deviation of D is approximately $0.0064D$.

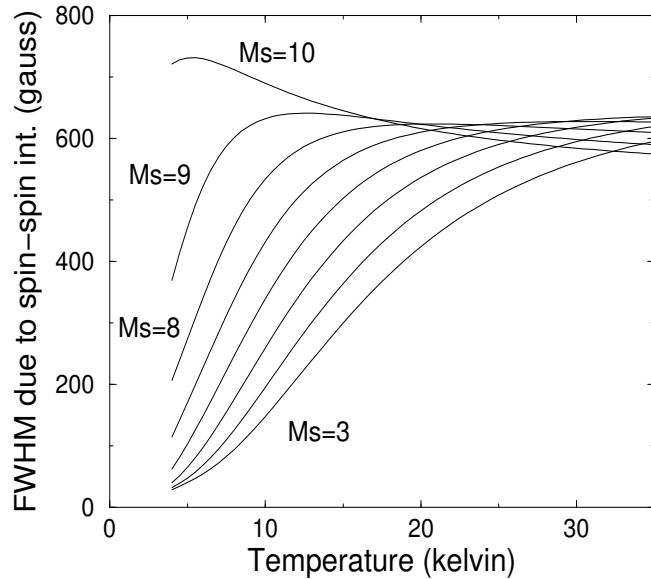


FIG. 5. Calculated FWHM caused by the spin-spin interactions only, shown vs temperature at $\nu = 116.9$ GHz for Fe_8 . Here the exchange constant J is -7 gauss, $\Gamma \equiv \sum'_{ij} A_{ij}^2/N = 86$ gauss 2 and $\Lambda \equiv \sum'_{ij} J_{ij} A_{ij}/N = -156$ gauss 2 .

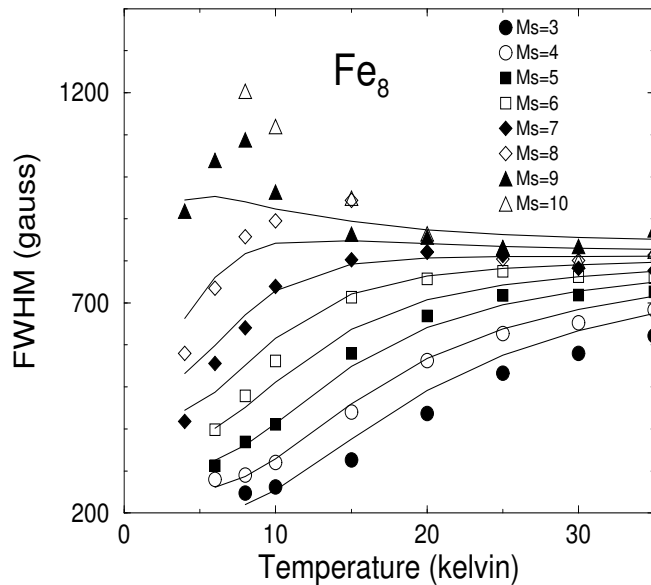


FIG. 6. Calculated (curves) and measured FWHM (symbols) vs temperature at $\nu = 116.9$ GHz for Fe_8 . Here we use the standard deviation of D , $\sigma_D \approx 0.0064D$, the exchange coupling constant, $J = -7$ gauss, $\Gamma = 86$ gauss 2 , and $\Lambda = -156$ gauss 2 . The solid curves, from bottom to top, correspond to $M_s = 3, 4, \dots, 9, 10$. See the text for possible sources of the discrepancy between theory and experiment for low temperatures and large M_s .

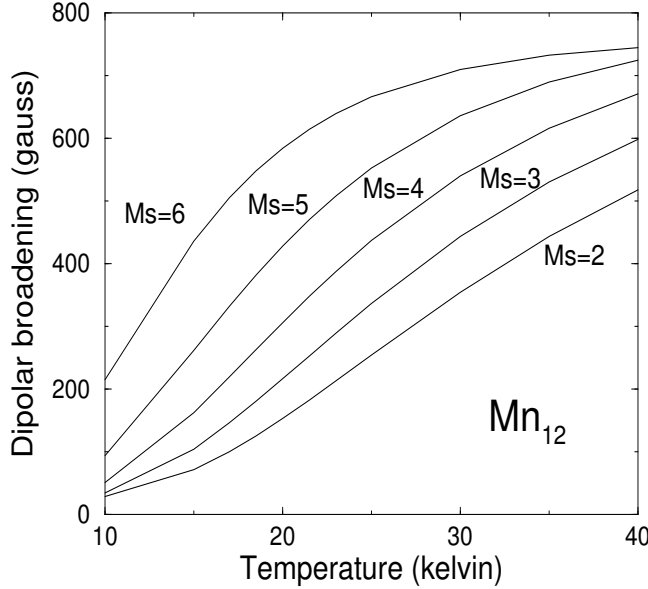


FIG. 7. Calculated FWHM for Mn_{12} caused by the dipolar interactions only, shown vs temperature, at $\nu = 189.123$ GHz, with the sum of the squared dipolar interactions $\Gamma = 203$ gauss 2 . The examined temperature range for Mn_{12} is from 10 K to 40 K.

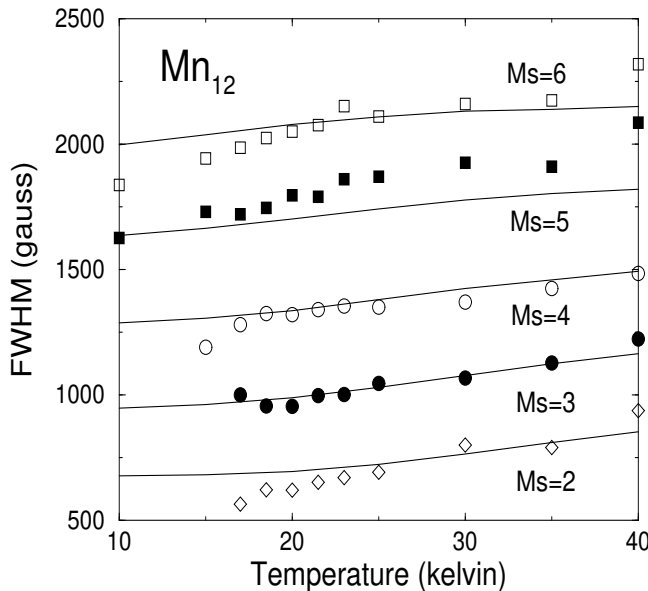


FIG. 8. Calculated (curves) and measured (symbols) FWHM vs temperature at $\nu = 189.123$ GHz for Mn_{12} . Here the D -strain ($\sigma_D \approx 0.018D$), g -strain ($\sigma_g \approx 0.002g$), and the dipolar interactions ($\Gamma \approx 203$ gauss 2) are included in the calculated linewidths.

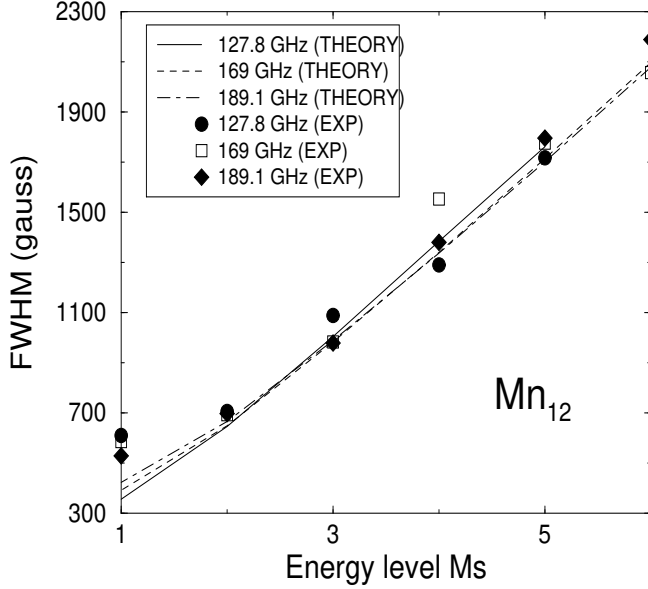


FIG. 9. Calculated (curves) and measured (symbols) FWHM vs energy level M_s at $T = 20$ K for $\nu = 127.8, 169$, and 189.1 GHz for Mn_{12} . Here the values of σ_D , σ_g , and Γ are the same as those in Fig. 8. Because of a relatively small contribution of the dipolar interaction to the linewidths, the linewidths do not change much with the resonance frequency.

TABLES

TABLE I. Optimum values of the parameters used in the line-shift and linewidth analysis. Here σ_D is the standard deviation of D , σ_g is the standard deviation of g , J is the exchange coupling constant between nearest-neighbor molecules (negative sign means ferromagnetic interaction), $\Delta \equiv \sum_{ij} A_{ij}/N$ which vanishes for spherical samples, $\Gamma \equiv \sum_{ij} A_{ij}^2/N$, and $\Lambda \equiv \sum_{ij} J_{ij}A_{ij}/N$. With experimentally determined values of D and g ,^{3,19} for Fe₈ we optimize J and Δ for the line shifts and σ_D , Γ , and Λ for the linewidths, while for Mn₁₂ we optimize σ_D , σ_g , and Γ for the linewidths.

	Fe ₈	Mn ₁₂
D	0.288 k_B	0.55 k_B
σ_D	0.0064 D	0.018 D
g	2.00	1.94
σ_g	—	0.002 g
J	−7 gauss	—
Δ	−20 gauss	—
Γ	86 gauss ²	203 gauss ²
Λ	−156 gauss ²	—